GPCRs through the keyhole: the role of protein flexibility in ligand binding to β-adrenoceptors

Abigail L. Emtage†*, Shailesh N. Mistry, Peter M. Fischer, Barrie Kellam, Charles A. Laughton

School of Pharmacy and Centre for Biomolecular Sciences, The University of Nottingham, University Park, Nottingham, NG7 2RD, UK.

Corresponding Author

* Email: Abigail.Emtage@nottingham.edu.my

Phone: +60 (0)3 8924 3646

Fax: +60 (0)3 8924 8018

Present Addresses

† School of Pharmacy, The University of Nottingham Malaysia Campus, Jalan Broga, 43500 Semenyih, Selangor, Malaysia.

GPCRs through the keyhole: the role of protein flexibility in ligand binding to β-adrenoceptors

G protein-coupled receptors (GPCRs) are proteins of pharmaceutical importance, with over 30% of all drugs in clinical use targeting them. Increasing numbers of X-ray crystal (XRC) structures of GPCRs offer a wealth of data relating to ligand binding. For the β-adrenoceptors (β-ARs), XRC structures are available for human β_2- and turkey β_1-subtypes, in complexes with a range of ligands. While these structures provide insight into the origins of ligand structure-activity relationships (SARs), questions remain. The ligands in all published complexed XRC structures lack extensive substitution, with no obvious way the ligand-binding site can accommodate β_1-AR-selective antagonists with extended side-chains *para*- to the common aryloxypropanolamine pharmacophore. Using standard computational docking tools with such ligands generally returns poses that fail to explain known SARs. Application of our Active Site Pressurization (ASP) modelling method to β-AR XRC structures and homology models however, reveals a dynamic area in the ligand-binding pocket that, through minor changes in amino acid side chain orientations, opens a fissure between transmembrane (TM) helices H4 and H5, exposing intra-membrane space. This fissure, which we term the 'keyhole', is ideally located to accommodate extended moieties present in many high-affinity β_1-AR-selective ligands; allowing the rest of the ligand structure to adopt a canonical pose in the orthosteric binding site. We propose the keyhole may be a feature of both β_1- and β_2-ARs, but that subtle structural differences exist between the two, contributing to subtype-selectivity. This has consequences for the rational design of future generations of subtype-selective ligands for these therapeutically important targets.

Keywords: GPCRs, beta adrenergic receptor, modelling, docking, active site pressurization, molecular dynamics, protein flexibility

Abbreviations: GPCR, G protein-coupled receptor; ASP, Active Site Pressurization; XRC, X-ray crystallography; β-AR, beta adrenergic receptor; T4L, T4 lysozyme; MD, molecular dynamics; TM, transmembrane; H1 – H7, helix number 1 through to 7; ECL, extracellular loop; ICL, intracellular loop; HBA, hydrogen bond acceptor; HBD, hydrogen bond donor; H-bond, hydrogen

bond; SAR, structure-activity relationship; LJ, Lennard-Jones; SEM, standard error of the mean; PDB, Protein Data Bank; VdW, Van der Waals

Introduction

The now rapidly-increasing number of XRC structures of GPCRs is providing a wealth of data about the structural basis of the mechanism of action of these pharmaceutically very important molecules and how this is modulated by ligand binding.(Congreve, Langmead, Mason, & Marshall, 2011; Heifetz et al., 2015; Katritch, Cherezov, & Stevens, 2012; B. K. Kobilka, 2007; 2011; Parrill & Bautista, 2010; Tate, 2012; Topiol & Sabio, 2009; Venkatakrishnan et al., 2013) In the case of β-ARs, we now have crystal structures available for the human β_2- and turkey β_1-ARs in complexes with a range of agonists, antagonists, inverse agonists (Table 1) and a series of ligand sub-fragments. In addition there are G-protein and nanobody-bound structures, as well as an oligomeric apo-receptor structure.(Bokoch et al., 2010; Cherezov et al., 2007; Christopher et al., 2013; Hanson et al., 2008; J. Huang, Chen, Zhang, & Huang, 2013; Miller-Gallacher et al., 2014; Moukhametzianov et al., 2011; Rasmussen et al., 2007; 2011a; 2011b; Ring et al., 2014; Rosenbaum et al., 2011; Wacker et al., 2010; Warne, Edwards, Leslie, & Tate, 2012; Warne et al., 2011; 2008; Weichert et al., 2014; Zou, Weis, & Kobilka, 2012) The holo/liganded structures reveal a consistent mode of interaction with the receptors whether the receptor is in its inactive (R) or active (R*) state (Figure 1). The orthosteric binding pockets of β_1- and β_2-ARs are almost identical. Of the amino acids that line the pocket the only difference evident is at position 7.35 (Ballesteros-Weinstein numbering(Ballesteros & Weinstein, 1995)) where Phe^{359} in β_1-AR is replaced by Tyr^{308} in β_2-AR.(B. K. Kobilka, 2011) The β_2-AR XRCs indicate that $Tyr^{308,7.35}$ can stabilise $Asn^{293,6.55}$ via interhelical H-bonding, whereas $Asn^{344,6.55}$ in β_1-AR does not have this stabilising feature and adopts a different rotamer position. As was

originally indicated by mutagenesis studies(Baker, Proudman, Hawley, Fischer, & Hill, 2008; Dixon et al., 1987; Strader et al., 1988; 1987; Strosberg, 1993), XRCs indicate that the essential ethanolamine core (coloured blue in Table 1 and Figure 1), present in all β-AR ligands with the exception of dobutamine and its sub-fragments, makes salt-bridge and hydrogen-bonded interactions with $Asp^{3.32}$ and $Asn^{7.39}$ respectively. (Cherezov et al., 2007; Christopher et al., 2013; Hanson et al., 2008; J. Huang et al., 2013; Miller-Gallacher et al., 2014; Moukhametzianov et al., 2011; Rasmussen et al., 2007; 2011a; 2011b; Ring et al., 2014; Rosenbaum et al., 2011; Wacker et al., 2010; Warne et al., 2008; 2011; 2012; Weichert et al., 2014; Zou et al., 2012) The ethanolamine nitrogen atom is protonated at physiological pH and the carbinol stereochemistry of the higher affinity isomer is as shown in Table 1. An extensive hydrogen-bonding network exists between the core and several further important residues (represented in Figure 1 as yellow arrows indicating the direction of H-bond donation). $Tyr^{7.43}$ plays a role in stabilising $Asp^{3.32}$ through an interhelical (H7-H3) H-bond (shown as a purple arrow), and has potential to interact with the core ethanolamine. *N*-Substituents of the ethanolamine ('tail' groups) extend in the general direction of the entrance channel towards the extracellular surface, while moieties attached to the carbinol side of the core pharmacophore ('head' groups) occupy a large and rather hydrophobic pocket in which $Phe^{6.52}$ and $Phe^{5.32}$ are often involved in π-stacking interactions and $Val^{3.33}$ is known to be important.(Bokoch et al., 2010; Chelikani et al., 2007; Cherezov et al., 2007; Christopher et al., 2013; Hanson et al., 2008; J. Huang et al., 2013; B. K. Kobilka, 2011; Lebon, Warne, & Tate, 2012; Moukhametzianov et al., 2011; Rasmussen et al., 2007; 2011a; 2011b; Rosenbaum et al., 2011; Wacker et al., 2010; Warne et al., 2008; 2011; 2012; Zou et al., 2012) The head group (coloured red in Tables 1 and 2 and Figure 1) largely determines whether

the ligand is an agonist or antagonist (for the conventional G-protein signalling pathway). Biogenic amines such as adrenaline possess a catechol head group (1,2-dihydroxyphen-4-yl) attached directly to the core ethanolamine, which forms H-bonds with $Ser^{5.43}$ and $Ser^{5.46}$ on H5, respectively. (Rasmussen et al., 2011a; 2011b; Ring et al., 2013; Rosenbaum et al 2011; Warne et al., 2011; Weichert et al., 2014) These interactions draw H5 inwards towards the core, reducing the pocket size, and stabilising the active (R*) signalling state of the receptor. In contrast, the addition of a methyleneoxy spacer between the ethanolamine and the aromatic portion of the head group (i.e. to furnish the aryloxypropanolamine scaffold), pushes the aromatic portion of the head group deeper into the binding pocket. This reduces the necessary inward conformational movement of the receptor to maximize interaction with this portion of the ligand, and/or does not induce the specific rotamer states of both $Ser^{5.42}$ and $Ser^{5.46}$ to fully facilitate movement of H5; resulting in an antagonist, inverse agonist, or partial agonist ligand. (Bokoch et al., 2010; Cherezov et al., 2007; Christopher et al., 2013; Hanson et al., 2008; J. Huang et al., 2013; B. K. Kobilka, 2011; Lebon et al., 2012; Moukhametzianov et al., 2011; Rasmussen et al., 2007; Wacker et al., 2010; Warne et al., 2008; 2011; 2012; Zou et al., 2012)

The R groups attached to the head group (Figure 1) represent the potential for structural diversity; heteroaromatic ring systems are common (see Table 1). The green line indicates conserved π-π stacking between $Phe^{6.52}$ and the common aromatic part of the head group, although if the ring system is larger, $Phe^{5.32}$ located on extracellular loop 2 (ECL2) can also contribute to π-π stacking (represented as dashed green line). Dashed yellow arrows indicate the general locations of previously observed ligand-dependent H-bonding between the β-ARs and antagonists (see references in Table 1 for details). The carbazole NH present in carazolol **(1)** and the indolic NH moieties of cyanopindolol

(2) and iodocyanopindolol **(3)** can donate H-bonds to Ser$^{5.42}$, whereas the benzofuran oxygen of **(8)** can also receive an H-bond from this residue. The nitrile groups of cyanopindolol **(2)** and iodocyanopindolol **(3)** can accept a weak H-bond from Thr$^{5.34}$ and Asn$^{6.55}$. Furthermore, Asn$^{6.55}$ can also form H-bonds with the morpholino oxygen of timolol **(6)** and ethoxy group of **(8).** The thiadiazole moiety present in timolol **(6)** can accept H-bonds from Thr$^{3.37}$. The R1 group, or tail group (coloured black), can be extremely short or long and diverse (see Table 1). Examples of the latter have been associated with biased receptor signalling (signalling mediated through pathways others than the G-proteins)(Liu, Horst, Katritch, Stevens, & Wuthrich, 2012; Warne et al., 2012) and subtype selectivity as longer tail groups have the potential to make interactions with the less conserved residues at the pocket entrance and extracellular surface of the receptor. (B. K. Kobilka, 2011)

Table 1. β-AR antagonist ligands that have been co-crystallised with a receptor to date.

Compound ID	**β-blocker ligands[a]**	**Structure (PDB codes)[b]**	**Resolution (Å)**	**Structure[c]**

(1)	Carazolol	Human β_2-AR-T4L construct (2RH1) Human β_2-AR-Fab construct (2R4R, 2R4S) Turkey β_1-AR construct (2YCW)	2.40(Cherezov et al., 2007) 3.40(Rasmussen et al., 2007) 3.00(Moukhametzianov et al., 2011)	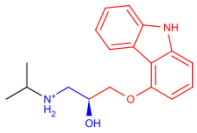
(2)	Cyanopindolol	Turkey β_1-AR construct (2VT4, 2YCX, 2YCY, 4BVN)	2.70(Warne et al., 2008), 3.25(Moukhametzianov et al., 2011), 3.15(Moukhametzianov et al., 2011), 2.10 (Miller-Gallacher et al., 2014)	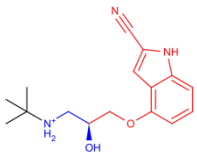
(3)	Iodocyanopindolol	Turkey β_1-AR construct (2YCZ)	3.65(Moukhametzianov et al., 2011)	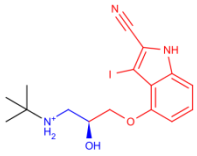
(4)	Bucindolol	Turkey β_1-AR construct (4AMI)	3.20(Warne et al., 2012)	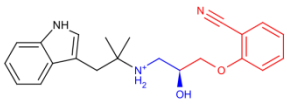
(5)	Carvedilol	Turkey β_1-AR construct (4AMJ)	2.30(Warne et al., 2012)	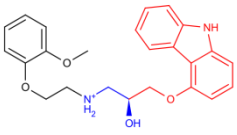
(6)	Timolol	Human β_2-AR-T4L construct (3D4S)	2.80(Hanson et al., 2008)	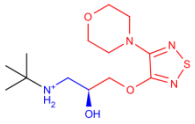

(7)	ICI-118,551	Human β_2-AR-T4L construct (3NY8)	2.84(Wacker et al., 2010)	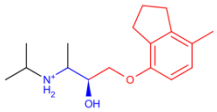
(8)	See Wacker *et al.*(Wacker et al., 2010) (inverse agonist)	Human β_2-AR-T4L construct (3NY9)	2.84(Wacker et al., 2010)	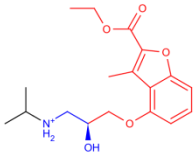
(9)	Alprenolol	Human β_2-AR-T4L construct (3NYA)	3.16(Wacker et al., 2010)	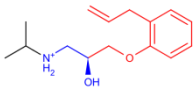

[a]Ligands which stabilise reduced-signalling or non-signalling states of β-ARs are classified as partial agonists, antagonists and inverse agonists; generally, they may be referred to as 'β-blockers'. They are also collectively referred to as antagonists within this manuscript.

[b]The ligands shown have been crystallised with engineered β-ARs

[c]The essential ethanolamine core of each ligand is coloured blue, the head group is coloured red, and the tail group is coloured black. All ligands are represented as the higher affinity *S*-enantiomers.

Although the XRC structure data thus gives invaluable insights into many aspects of the SARs of β-AR ligands, it does not explain everything. In particular, there are a number of antagonists that feature longer head group extensions than any of the ligands in published crystal structures. Examples are acebutolol **(10)**, betaxolol **(11)**, esmolol **(12)**, bisoprolol **(13)**, CGP20712A **(14)**, LK 204-545 **(16)**, and 1-(2-(3-(4-(2-(cyclopropylmethoxy)ethoxy)phenoxy)-2-hydroxypropylamino)ethyl)-3-(4-hydroxyphenyl)urea **(15)**(Mistry et al., 2013); these are shown in Table 2.

Table 2. "Extended" antagonist structures that exhibit mild to moderate β_1-AR selectivity

Compound ID	**β-blocker ligands**	**Human β_1-AR/β_2-AR selectivity: ^{3}H-CGP12177 whole-cell binding affinities (log Kd)** (Baker, 2005; 2010; Wacker et al., 2010)			**Structure[a]**
		β_1-AR affinity	**β_2-AR affinity**	**Ratio β_1:β_2**	

(10)	Acebutolol	-6.46	-6.08	2.4	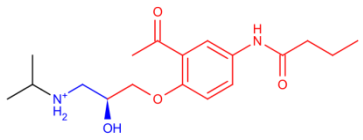
(11)	Betaxolol	-8.21	-7.38	6.8	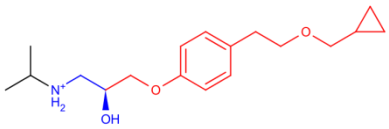
(12)	Esmolol	-6.73	-5.73	10	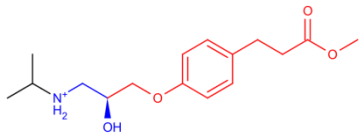
(13)	Bisoprolol	-7.83	-6.70	13.5	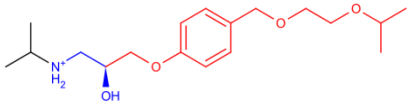
(14)	CGP20712A	-8.81	-6.11	501.2	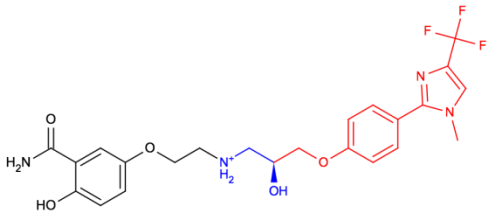
(15)	See Mistry *et al.*(Mistry et al., 2013)	-7.59	-4.65	871.0	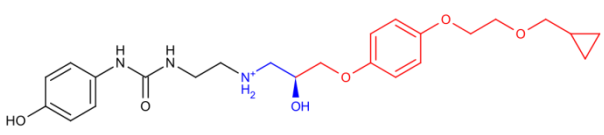

(16)	LK 204-545	-8.38	-5.00	2398.8	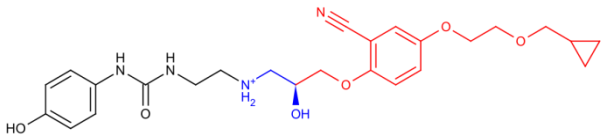

[a]The ethanolamine core of each ligand is coloured blue, the head group is coloured red, and the tail group is coloured black.

One particular feature of many of these ligands is their increased selectivity, compared to less extensive ligands, for the β_1-AR over the β_2-AR (Table 2). As part of our studies into the design and development of subtype-selective ligands, we attempted to dock these molecules to the known β-AR XRC structures, and homology models of the human β_1- and β_2-AR that we have built from them. In all cases, using conventional docking methods (Glide), we found it almost impossible to generate poses for these ligands that resembled the canonical one, due to the inability of the extended ligand head groups to fit within the confines of the conventional binding pocket. Many of the poses generated failed to show convincing interactions for the ethanolamine core and failed to explain other aspects of known SARs. On this basis we concluded that it was worth investigating an alternative hypothesis for the activity of such ligands – not that they adopted an alternative pose in the β-AR ligand binding site, but that this site in fact has as-yet unrecognised structural plasticity and can distort to accommodate the ligands whilst allowing them to maintain an otherwise conventional pose.

We envisaged that our Active Site Pressurization (ASP) method (Withers, Mazanetz, Wang, Fischer, & Laughton, 2008) would be ideal for this investigation. ASP simulates the process of injecting particles into a protein cavity rather like injecting a resin into a mould. The injection process takes place under pressure, so once the empty

volume is filled, further expansion can take place in the most energetically favourable directions. The method does not involve making any prior decisions as to what the modes of deformation might be, nor does it require one to make any assumptions as to the size or shape of the molecule that will fit into the volume. Here we present the results of that study.

Remarkably, our findings suggest that the hydrophobic pocket in both the β_1- and β_2-AR contains a weak point in its wall between H4 and H5, such that ASP leads to the creation of a fissure in the pocket that leads out to the intra-membrane space. This fissure, which we term the 'keyhole', has exactly the position, dimensions, and chemical characteristics to permit ligands with extended head groups to bind to the receptors in the canonical orientation. Indeed, several of the β-AR XRC structures corroborate our ASP findings. Though not specifically mentioned by the authors of the publications, 11 of the 16 β_1-AR structures and 1 of the 16 β_2-AR structures do in fact exhibit a keyhole, as a result of minor side-chain and backbone adjustments which to a large extent are as predicted by our ASP studies.

One of the few residues within 5 Å of the conventional binding pocket that is not conserved between the β_1- and β_2-AR is located at position 4.56 (Val^{189} and Thr^{164} in β_1- and β_2-AR respectively) and is one of five main residues which line the keyhole; it also happens to be the site of the naturally occurring β_2-AR Thr^{164}Ile polymorphism.(Green, Cole, Jacinto, Innis, & Liggett, 1993) This mutation results in reduced agonist affinity and slightly lower receptor basal activity.(Green et al., 1993; Green, Rathz, Schuster, & Liggett, 2001) Our findings suggest that this residue may well play an important role in ligand selectivity.

Methods

1. Homology modelling

Homology models were built using Prime(Green et al., 1993; 2001; Suite 2012: Prime, version 3.1, Schrödinger LLC New York, NY, 2012) and refined using Maestro(Suite 2012: Maestro, version 9.3, Schrödinger, LLC, New York, NY, 2012) and the Prime loop refinement module(Jacobson, Friesner, Xiang, & Honig, 2002; Jacobson, Pincus, & Rapp, 2004). The β_2-T4L construct containing the ligand carazolol **(1)** (PDB code 2RH1) was reverse engineered to more accurately represent the human β_2-AR wild-type sequence; chain B of the 2YCW XRC structure was used to model the human β_1-AR sequence as it also contains carazolol **(1)**, and despite being a thermostabilised avian construct (β36-m23(Jacobson et al., 2002; 2004; Moukhametzianov et al., 2011)) with slightly different pharmacology to the human β_1-AR,(Baker, Proudman, & Tate, 2011) it shares higher homology with human β_1-AR than human β_2-AR (2RH1) does. The wild-type human β_1-AR and β_2-AR sequences were obtained from NCBI(National Center for Biotechnology Information. Protein Database) and aligned to both crystal templates (2RH1 and 2YCW) using Prime. The alignment was checked using ClustalW(Larkin et al., 2007) and found to be in good agreement. The N-terminus of the β_1-AR sequence was truncated by 49 residues, and 84 residues were removed from the C-terminus. Due to the limitations of loop modelling tools, no attempt was made to model the full length of the third intracellular loop, rather 45 residues were removed and the ends (Asp^{259} and Arg^{305}) were joined to form a pseudo-loop. For β_2-AR the Asn^{187}Glu mutation in ECL2, which had been employed to eliminate a glycosylation site in the β_2-T4L crystal construct, was reversed, the T4-lysozyme was removed and the third intracellular loop was replaced. This loop, despite being long, is still

considerably shorter than that of the β_1-AR isoform, and was successfully modelled using Prime's ultra-extended loop refinement tool with the addition of an Atom Specification Language (ASL) placed implicit membrane to exclude predictions that were not outside the membrane region. Unresolved N- and C-terminal regions were omitted as with the β_1-AR model, resulting in a β_2-AR model that spanned from Thr^{25} to Cys^{393} (inclusive). The template ligand carazolol **(1)** was preserved in both models but no water molecules or other heteroatoms were retained or added.

2. Active Site Pressurization

ASP was performed using the approach described by Withers *et al.*,(Withers et al., 2008) re-implemented in code written in the modelling language NAB.(Macke & Case, 2009) Grids for the insertion of the Lennard-Jones (LJ) particles were built, with a 1.1 Å spacing, to encompass the region occupied by the carbazole group present in carazolol **(1)**, plus a 7.0 Å margin along all axes beyond it. The starting seed particle from which the LJ cast grew outwards was chosen to correspond to the ether oxygen atom of carazolol **(1)** before the ligand was removed. The Amber ff99SB force field (Hornak et al., 2006) was used to parameterise the protein; default protonation states were used: though there are suggestions that certain residues may exist at non-standard states,(Fahmy et al., 1993; Cherezov et al., 2007; Vanni, Neri, Tavernelli, & Rothlisberger, 2009; 2011) the ASP method is not expected to be sensitive to this as the residues in question ($Asp^{2.50}$ and $Glu^{3.41}$) are not in close proximity with the binding cavity and ASP particles are uncharged Lennard-Jones spheres, so it is unlikely that utilising the non-standard states would alter the strength of relevant interactions,. For all ASP runs the C^{α}-atoms of the protein were restrained to their initial positions with a force constant of 10.0 kcal/mol/$Å^2$. ASP runs consisted of an initial energy

minimisation step of 100 cycles, an equilibration molecular dynamics (MD) phase (between 0.2 and 2 ps), and finally the inflation phase with one ASP particle insertion step every 0.2 ps of dynamics (equal to 20 ps of MD in total for a run of 100 ASP cycles). Replicates (10 per system) of the ASP simulations differed only in the length of the initial equilibration phase.

While these initial ASP studies were the ones that led to the discovery of the keyhole fissure that formed between helices 4 and 5, the non-selective pressurization of the whole ligand-binding cavity also led to other regions of the binding cavity, in particular the vital $Asp^{3.32}$ and $Asn^{7.39}$ side chains, adopting rotamers no longer conducive to ligand binding, having being pushed aside as the pocket filled with LJ particles. Therefore a focused ASP methodology was subsequently employed to specifically probe the keyhole region. This second application of ASP employed the original version of the algorithm, where a 14 x 10 x 10 Å grid was placed, covering the area from the inner edge of the conventional pocket to the outside of helices 4 and 5, encompassing the residues where movement involved in the formation of the fissure had previously been observed. The seed particle for this focused ASP grid corresponded with carazolol's **(1)** carbazole nitrogen atom. All other parameters were the same as in previous ASP runs (four replicates per system).

3. Docking

Docking was carried out using Glide. (Friesner et al., 2004; Suite 2012: Glide, version 5.8, Schrödinger, LLC, New York, NY, 2012) Structures of all ligands in Table 1 and Table 2 were drawn in Maestro's 2D sketcher and prepared with LigPrep(Suite 2012: LigPrep, version 2.5, Schrödinger, LLC, New York, NY, 2012) to produce the *S*-enantiomer carbinol group, and protonated nitrogen within the core ethanolamine (the additional chiral centre present in ICI-118,551 **(7)** was generated as both *S* and *R*).

Crystal structures were imported and prepared minimally (processed, water removed, not refined) with Maestro's protein preparation wizard. Using Glide, grids were produced based on the centre of carazolol **(1)** – this differed slightly depending on the crystal/model template; the relevant carazolol **(1)** molecule was used to select the centre for each grid. The grids each had a 10 $Å^3$ inner box based around the carazolol **(1)** centre, with an outer box of 38 $Å^3$. Docking of all previously crystallised antagonist ligands (Table 1) to our models was first performed with no constraints and in several cases yielded poor results with few poses reflecting crystallographic ligand placement. Subsequently, a core constraint was defined which required that ligands dock within 2.0 Å of the ethanolamine heavy atoms of each model's cognate carazolol **(1)** molecule. This constraint was successful in producing poses highly similar to crystallographic data for each ligand and was implemented for all future docking. Extended Sampling was turned on, for each ligand 50 poses were minimised post-docking and a maximum 20 poses output. Default settings were used unless otherwise stated.

4. Molecular Dynamics

Selected ligand poses were refined using MD methods with AMBER 11.(Case et al., 2005; Pearlman et al., 1995) For this work all the ligands in Table 2 along with carazolol **(1)** were parameterised using the AMBER Antechamber utility(J. Wang, Wang, Kollman, & Case, 2005), partial charges being calculated using the AMI-BCC method(Jakalian, Bush, Jack, & Bayly, 2000; Jakalian, Jack, & Bayly, 2002). The protein was parameterised as for the ASP studies. All complexes underwent a steepest decent minimisation for 50 cycles before switching to the conjugate gradient method until the convergence criterion of 0.1 kcal/mol-Å was reached. MD simulations were then run for 10 ns each, utilising a 2.0 fs time step and implementing the SHAKE algorithm for all bonds to hydrogen. Solvent was described implicitly via a generalised

Born model (Onufriev model, igb=5).(Onufriev, Bashford, & Case, 2000; 2004) The membrane was not described since Amber 11 does not have an implicit membrane option; instead the seven transmembrane (TM) helical regions of the protein backbone were restrained (restraint weight 0.1 kcal/mol- $Å^2$). A Langevin dynamics setting of 5ps $^{-1}$ and a non-bonded cut off of 25.0 was used. The MMPBSA utility within Amber was employed to calculate MM-GBSA free energies of binding for each receptor-ligand complex over the course of each 10 ns simulation, sampling at intervals of 0.1 ns.

Results

1. Homology models

Homology models were checked using PROCHECK(Laskowski, MacArthur, Moss, & Thornton, 1993) and Molprobity. (Davis et al., 2007) All models showed few outliers in Ramachandran plots (Supplementary Information Table S1); all of these outliers were found to be in intra- or extra-cellular loop regions far from the binding site. This finding is consistent with the template crystal structures, which also showed outliers, especially in the third intracellular loop. Due to the extremely high level of conservation between template binding sites (and subsequently models) we believe the models to be accurate enough for prediction of antagonist binding modes.

2. Initial docking attempts

When core constraints were used, we were able successfully to re-dock, using Glide, carazolol **(1)** and all other (Table 1) cognate ligands trialled to the 2RH1 and 2YCW crystal structures, as well as the homology models of both the β_1- and β_2-AR (Figure 2a). H-bonding criteria were defined as a maximum H-X distance of 2.5 Å, a minimum donor angle of 90 ° and a minimum acceptor angle of 60 °. All top poses showed four

H-bonds between the core ethanolamine and the conserved Asp$^{3.32}$ and Asn$^{7.39}$ residues. The top scoring pose for each ligand was in most cases nearest to the crystallographic pose, as defined by manual superimposition of previously aligned XRCs (See Figure 2a and Supplementary Information Table S2 for GlideScores). H-bonding to S$^{228, 5.42}$ is not shown in the β_1-AR model in Figure 2a (due to slightly unfavourable geometry, although proximity is good), but was seen in the β_2-AR model, as with the XRC structures.

However, when the same protocol was used for extended head group ligands (Table 2), we were unable to generate convincing poses consistently. In some cases the requirement that the core constraint be satisfied resulted in no docking poses at all being returned; when poses were produced they commonly exhibited fewer H-bonds between the ligand core ethanolamine and the Asp$^{3.32}$ and Asn$^{7.39}$ residues, and adopted either what we term 'U-shaped' or 'reversed' poses (See Supplementary Information Table S3 for GlideScores). U-shaped poses (Figure 2b) are defined as a potential binding mode in an XRC or XRC-based model in which both the head and tail ends of the ligand are positioned towards the binding cavity entrance and extracellular surface of the β-AR, often in solvent-accessible regions and not fully utilising the deeper, hydrophobic part of the binding cavity, which the head groups of all ligands in Table 1 occupy. Reversed poses (see Supplementary Information Figure S1) are defined as those in which the tail group is orientated towards the serine residues on H5, and the head group occupies the pocket entrance.

U-shaped poses were produced for all extended ligands except CGP20712A (**14)** in the β_2-AR model, but in the β_1-AR model U-shaped poses were only obtained for LK 204-545 **(16)** and esmolol **(12)**, all other ligands failed to dock. In this docking mode, we typically saw the extended ligand head groups engage in H-bonding interactions

with Asn$^{6.55}$ (Figure 2b) or the backbone of Thr$^{5.34}$ on ECL2, with the longer extensions terminating in the vicinity of Arg/Asp$^{7.27}$ (β_1-AR Arg^{351}, β_2-AR Asp^{300}) at the extracellular surface. The tail groups of the longer ligands LK 204-545 **(16)** and **(15)** made contacts with the backbone of Phe$^{5.32}$ (situated in ECL2) in the β_2-AR model, and the terminal hydroxyl group of LK 204-545 **(16)** H-bonded to Asp$^{356, 7.32}$ in the β_1-AR model. The equivalent of this latter interaction was not seen in the β_2-AR as the residue at the corresponding position is Lys^{305}, which forms a salt bridge with Asp$^{192, 5.31}$ across the entrance to the binding pocket.

Reversed poses were most commonly seen with CGP20712A **(14)**, which failed to produce any canonical or U-shaped poses when core constraints were utilised, instead preferring to dock in this reversed orientation in both the crystal structures and β_2-AR receptor model, and not at all in the β_1-AR model or XRC. The bi-aryl nature of this ligand's head group is inherently less flexible than the corresponding alkoxy head group of a ligand like LK 204-545 **(16)** or **15**, so a U-shaped pose would not necessarily be expected/possible. Reversed poses were not seen with LK 204-545 **(16)**, despite its structural similarity to compound **15** for which a single reversed pose was produced in the β_1-AR model when core constrains were removed (see Supplementary Information Figure S1).

To explore the possibility that these extended ligands actually adopt a significantly different, but consistent binding pose compared to the established ligands, the docking procedure was repeated without the core constraints. The result was that the extended (Table 2) ligands rarely made contacts with the conventional binding site but instead showed interactions with residues at the edge of the pocket and extracellular surface, with major inconsistencies between poses adopted by structurally closely related ligands (such as the reversed pose seen for ligand **15** but not for LK 204-545

(16)). The general absence of contacts deemed vital by SAR, mutation studies, and current structural knowledge from crystallography, suggested these non-core-constraint poses were unlikely to be valid.

3. Active Site Pressurization

ASP was applied to the homology models of both the β_1- and β_2-AR. In the first instance simulations were repeated ten times to assess the significance and reproducibility of structural perturbations that were observed. In the majority of cases, after an initial phase when the empty volume of the pocket was filled, ASP particles then pushed open a narrow fissure between H4 and H5 exposing the intra-membrane space (Figure 3). The fissure, which we have termed the 'keyhole', is formed by the adjustment of certain amino acid side-chain torsions with only minor adjustments to backbone atoms. In particular we observed movement of $Tyr^{5.38}$, $Ser^{5.42}$, $Ser^{5.46}$, $Val/Thr^{4.56}$, and to a smaller extent $Pro^{4.50}$ (see Supplementary Information Tables S4 and S5 for backbone C_{α} movement distances and side chain $\chi 1$ dihedral angles pre- and post-ASP). The residues newly accessible to the binding pocket comprise generally hydrophobic transmembrane amino acids (as they are located in intra-membrane space) including $Ala^{5.41}$, $Val^{5.45}$ (this residue is Ile^{214} in the turkey β_1-AR), as well as the indole ring of $Trp^{4.35}$.

In order to check that this observation was not an artefact of the homology modelling process, it was also applied to the crystal structures (2RH1 and 2YCW) with very similar results. The ASP methodology was refined to retain the integrity of the main binding pocket, thus creating the keyhole without distorting the vital $Asp^{3.32}$ and $Asn^{7.39}$ side chains required for ligand binding. These simulations were repeated four times for each receptor, replicate runs varying in the length of the equilibration MD

phase before ASP was begun (see Methods Section 2), in order to start from slightly varying initial structures and velocity distributions. We observed keyhole formation 100% of the time for the β_1-AR model, 50% of the time for the β_2-AR model, 50% for the 2YCW (turkey 'β_1-AR' β36-m23) XRC structure, and 75% of the time for the 2RH1 XRC structure. This suggests that keyhole formation from the β_1-AR model was less affected by fine details of the starting conformation of the receptor and particle insertion process than was the β_2-AR – features which may in turn relate to the entropic component of the free energy of keyhole formation in these two receptors. The model with the largest keyhole (defined visually in PyMOL (The PyMOL Molecular Graphics System, version 1.5.0.4, Schrödinger, LLC) using a surface representation with a default probe radius of 1.4 Å) was selected for each receptor to be used in post-ASP docking studies.

4. Docking studies after ASP

Glide was used to re-dock the extended ligands in Table 2: acebutolol **(10)**, betaxolol **(11)**, esmolol **(12)**, bisoprolol **(13)**, CGP20712A **(14)**, **(15)** and LK 204-545 **(16)**, to the β_1- and β_2-AR models featuring the keyhole. For consistency with the earlier studies, these docking runs used the same restraints on core interactions (see Methods Section). Although not always a high-scoring pose (see Supplementary Information Table S6 for GlideScores), in several cases a model was obtained in which simultaneously the extended head group moiety was located in the keyhole region, whilst the ethanolamine core was involved in the canonical interactions with $Asp^{3.32}$ and $Asn^{7.39}$ (Figures 4 and 5).

Ligands LK 204-545 **(16)** and **(15)** differ only in the presence of a cyano substituent on the aromatic ring in the former, yet the result of this addition is a

significant increase in β_1-AR binding affinity (-log Kd increased from -7.59 to -8.38, see Table 2). The docked poses for these ligands provide a plausible explanation for this (Figure 5). We see that the cyano group is placed in close proximity to $Asn^{6.55}$ and the possibility of a favourable hydrogen bonding interaction between these two would be enhanced even further if the asparagine were to adopt one of the alternative rotamers that have been observed experimentally in β_1-AR crystal structures.(Laskowski et al., 1993; Warne et al., 2011; 2012)

5. Evaluation of U-shaped versus keyhole poses by molecular dynamics.

To explore further the relative merits of the U-shaped versus keyhole pose options, selected models for all ligands in Table 2 in complex with both β_1-AR and β_2-AR receptors were refined using AMBER. As far as possible, all simulations began from poses generated from the docking procedures; where no suitable start-point was available, ligands were manually docked into the appropriate β_1- or β_2- model using data from cognate ligands in cognate protein models. The MD runs were stable and in all cases the ligand stayed within the pocket/keyhole while always retaining H-bonding contacts between the ligand core ethanolamine and the $Asp^{3.32}$ and $Asn^{7.39}$ clamp. See Supplementary Information Figure S2 for a summary of all β-AR residues implicated in H-bonding interactions.

5.1. H-bonding interactions between the ligand head/tail groups and the β-ARs observed during MD

a) The β_1-AR models

In addition to interactions with the core ethanolamine moiety, interactions commonly maintained between the β_1-AR models and ligands in U-shaped poses included H-

bonding between polar atoms in head group extensions and Asn$^{6.55}$ (acebutolol **(10)**, bisoprolol **(13)**, betaxolol **(11)** and **15**), Arg$^{7.27}$ (acebutolol **(10)** and esmolol **(12)**), and the backbone of Thr$^{5.34}$ (esmolol **(12)**), residues which were all seen to be involved in H-bonding interactions in the original docking results. New H-bonding interactions between head groups and Lys$^{6.58}$ (esmolol **(12)**) and the phenol of Thr$^{5.34}$ (bisoprolol **(13)**, betaxolol **(11)**, esmolol **(12)**, **15** and LK 204-545 **(16)**) were also observed during MD runs. The longer tail group of LK 204-545 **(16)** moved so as to create H-bonding opportunities between its urea carbonyl and Trp$^{7.40}$, and as seen in the original docking, the phenolic oxygen was also occasionally able to accept an H-bond from the non-conserved Arg$^{7.33}$. Ligand **15**, despite possessing a tail group identical to that of LK 204-545 **(16)**, failed to demonstrate any consistent H-bonding to/from its tail.

In contrast, when ligands were bound to the β_1-AR utilising the keyhole region, the same tail group showed interactions with the backbone of Phe$^{5.32}$ (**15** and LK 204-545 **(16)**). Ligand **15** also made the additional H-bonds to the conserved residues Trp$^{7.40}$, Asp$^{7.31}$, Gly$^{2.61}$, and Cys$^{5.30}$ (backbone carbonyl). LK 204-545 **(16)** formed H-bonds to Arg$^{7.33}$ (seen in the original docking and U-shaped MD complexes) demonstrating that keyhole binding does not preclude this subtype-specific tail group interaction, which likely confers some of the β_1-AR selectivity of this molecule. In the keyhole complexes the head groups of all extended ligands tended to H-bond directly with the keyhole residues Tyr$^{5.38}$, Ser$^{5.42}$, and Ser$^{5.46}$. All ligands, at some stage in the simulation, showed an interaction with either Ser$^{5.46}$ or Tyr$^{5.38}$, acebutolol **(10)** interacting with both of these simultaneously, due to its amide moiety (other ligands contain ether or ester moieties in the corresponding position).

b) The β_2-AR models

In the β_2-AR model the U-shaped poses showed head groups interacting with Thr$^{5.34}$ (side chain and backbone) and Asn$^{6.55}$, as with the β_1-AR. The ether moiety of esmolol **(12)** showed a brief interaction with the non-conserved Tyr$^{7.35}$ (Phe^{359} is the corresponding residue in the β_1-AR), but no equivalent to this ligand's interaction with Lys$^{6.58}$ in the β_1-AR was seen in the β_2-AR (where the corresponding residue is His^{296}). The phenolic oxygen atom in the tail group of **15** occasionally interacted with Trp$^{7.40}$. LK 204-545 **(16)** exhibited consistent interactions between its tail group urea moiety and the conserved Asp$^{5.31}$ in ECL2, potentially disrupting (or augmenting) the salt bridge formed by this residue with Lys$^{7.32}$ in the β_2-AR.

The β_2-AR keyhole complexes also showed consistent H-bonding interactions between ligand head groups and Tyr$^{5.38}$, Ser$^{5.42}$, and Ser$^{5.46}$. In the keyhole–LK 204-545 **(16)** complex tail group interactions with Lys$^{7.32}$ (Asp^{356} in the β_1-AR), Asp$^{5.31}$, Cys$^{5.30}$ and His$^{2.64}$ (Ile^{118} in the β_1-AR) were observed. The keyhole-**15** complex showed interactions between Trp$^{7.40}$ and Gly$^{2.61}$ and this ligand's tail group.

It is now generally accepted that the variability of the extracellular receptor surface is responsible for the different binding profiles of antagonists between these the β-AR subtypes (including turkey β_1-AR versus human β_1-AR). Binding and dissociation studies pay particular attention to the β_1-AR subtype specific Glu^{205} (ECL2) – Arg$^{351,7.27}$ salt bridge (not observed in turkey β_1-AR as Glu^{205} is Gln^{188} in this subtype and is between 3.5 – 10 Å away from Arg$^{7.27}$ in XRC structures) and the β_2-AR specific Asp$^{193,5.31}$ – Lys$^{305,7.32}$ salt bridge, the latter of which spans the entrance to the binding cavity of the β_2-AR, hindering unbinding and stabilising the inactive conformation of the β_2-AR(Bokoch et al., 2010; Davis et al., 2007; González, Perez-Acle, Pardo, & Deupi, 2011; Selvam, Wereszczynski, & Tikhonova, 2012). Although

we observe the tail groups of the ligands LK 204-545 **(16)** and **15** interacting with the Lys/Asp salt bridge at the entrance of the β_2-AR pocket, it is not obvious which of the observed binding modes is most likely. We observed ligand tail groups positioned either side of the salt bridge, occasionally interacting with Lys$^{7.32}$ or Asp$^{5.32}$ directly. Interestingly these same tail groups showed interactions with the equivalent residue to Lys$^{7.32}$ on the β_1-AR (Asp $^{356,7.32}$) as well as with the conserved Asp $^{5.32}$, and additionally with Arg $^{351,7.27}$ of the β_1-AR salt bridge. Variations of placement of the methoxyphenyl tail group of full agonist carmoterol are seen in monomer A and B of the β_1-AR crystal containing this ligand (due to a crystal contact in monomer A), suggesting that very small variations in backbone conformation can result in maintenance of the core ethanolamine binding site (and allow the core to dock) whist significantly affecting ligand tail placement. Our data suggest that tail groups have more freedom of movement generally as they tend to be orientated towards the extracellular entrance to the binding pocket, and do not stay anchored to a particular contact but move between several HBA/HBDs. Tail groups clearly play an important role in selectivity, due to their ability to make interactions with non-conserved extracellular surface residues.

5.2. Energetic analysis of alternative binding models

Using data from the last 10 ns of the simulation of each protein-ligand complex, the Amber11 MM-GBSA method was used to estimate free energies of binding. The results are shown in Table 3. The β_1-AR model containing the U-shaped betaxolol **(11)** pose failed to give a realistic free energy measure due to an unreasonably high VdW term (clashes between the ligand and receptor). CGP20712A **(14)** is not included in the data set as no U-shaped poses could be generated for this ligand.

Table 3. Energetic comparison of U-shaped and keyhole poses in β-ARs.

Ligand	U-shaped pose				Keyhole pose			
	β_1-AR model	SEM[b]	β_2-AR model	SEM	β_1-AR model	SEM	β_2-AR model	SEM
Acebutolol **(10)**	**-32.38**	0.55	**-45.41**	0.47	**-53.83**	0.43	**-56.13**	0.44
Betaxolol **(11)**	-	-	**-47.00**	0.60	**-57.32**	0.56	**-62.03**	0.44
Bisoprolol **(13)**	**-56.47**	0.58	**-60.68**	0.74	**-61.57**	0.46	**-66.58**	0.40
Esmolol **(12)**	**-44.16**	0.40	**-49.46**	0.47	**-48.69**	0.43	**-50.89**	0.52
LK 204-545 **(16)**	**-64.53**	0.61	**-60.53**	0.56	**-64.19**	0.59	**-70.00**	0.55
15	**-61.66**	0.50	**-65.45**	0.63	**-64.40**	0.54	**-70.49**	0.42

[a]MM-GBSA estimations of the free energy of binding for each complex. Energies in kcal/mol.

[b]SEM; standard error of the mean. SEM is used as the data from each snapshot of the simulation is considered when computing the MM-GBSA free energy estimation.

While, experimentally, all these ligands are β_1-AR-selective (Baker, 2005; Benfield & Sorkin, 1987; S. N. S. Louis, Nero, Iakovidis, Jackman, & Louis, 1999; Mistry et al., 2013), the MM-GBSA free energies of binding are almost always more favourable for the β_2-AR. Though this suggests the approach has neglected an isoform-specific energy term, it does not alter the key observation that the MM-GBSA scores clearly support the idea that the keyhole poses are more favourable energetically. In fact, the only case where a U-shaped pose scores more highly than a keyhole pose is in the case of the β_1-AR model complexed with LK 204-545 **(16)**, but the difference is not significant when the standard error of the mean is considered. The relative energetic cost of creating a keyhole in β_1-AR versus β_2-AR may also play a role in selectivity, but this cannot be

reported quantitatively here as the bulk solvent terms that come with the use of implicit solvent (as was the case for all ASP and subsequent MD studies) results in an energetic analysis that contains insufficient detail; we do note though (see section 3 above) that keyhole formation using ASP appears easier to initiate from the closed state of the β_1-AR than the β_2-AR.

Discussion

The application of the ASP process to both crystal structures and homology models of β_1- and β_2-ARs provides clear support for our hypothesis that the ligand binding cavity has the necessary plasticity to accommodate ligands bearing longer head groups than are present in any of the structures crystallised to date, without the need to propose a radically different binding mode. Remarkably, the 'keyhole' revealed by ASP, located between TM H4 and H5, is ideal in terms of location, size and chemical composition to accommodate these extended ligands. The polar groups (often ethers) of all ligands with extended head groups are well placed to engage in polar interactions and H-bonds with Ser $^{5.42}$, Ser $^{5.46}$ and Tyr $^{5.38}$ which line the keyhole, while the terminal isopropyl or cyclopropyl group occupies a hydrophobic patch at the surface of the protein in the intra-membrane space. These hydrophobic interactions are maximized in the β_1-AR subtype due to the valine residue at position 4.56, which lines the keyhole; a polar threonine residue exists at this position in the β_2-AR subtype.

Additional evidence for 'keyhole' formation at the H4/H5 interface in the β-ARs has come from molecular dynamics studies by other authors who have investigated binding and unbinding of ligands from GPCRs. Wang and Duan have used RAMD simulations to predict the exit pathway of carazolol **(1)** from the β_2-AR (T. Wang &

Duan, 2009). The authors identify a pathway between H4 and H5 as the second most common egress route, second only to the extracellular surface opening (carazolol **(1)** used this route 20% and 27% of the time in the two data sets). In a separate study by the same authors, this point of egress was also seen as the primary exit pathway for the ligand retinal in simulations of inactive bovine rhodopsin (T. Wang & Duan, 2007) Other intra-membrane egress pathways (between H1 and H7, and between H5 and H6) have also been determined for the ligand-free opsin,(Hildebrand et al., 2009; T. Wang & Duan, 2009) but were not observed in the β-ARs.(González et al., 2011; T. Wang & Duan, 2007) An impressive study of spontaneous binding of several β-blockers to the β_2-AR from 82 MD simulations between 1-19 μs in length, did not show any of the ligands actually entering the binding pocket via an intra-membrane route, but confirmed the results of other dynamical studies which identified the extracellular opening as the route of ligand entry(Dror et al., 2011; Hildebrand et al., 2009).

All crystal structures of the β-ARs exhibit only moderate-weak hydrophobic interactions at this helical interface, and although not always as large as the keyhole produced by ASP, 12 of the 32 currently availably β-AR XRCs display a cavity or hole in the binding pocket wall at this position (see Supplementary Information Table S7). We also know that there is a great deal of conformational flexibility possible in the area of the keyhole associated with receptor activation - β_2-AR structures show a 2.1 Å movement of the C_α of Ser $^{5.46}$ when agonist and antagonist structures are compared (a difference of ~1 Å in the β_1-AR turkey structures(González et al., 2011; Warne et al., 2011)). We also observe various rotamer states of Ser $^{5.46}$ depending on whether it can directly H-bond to the ligand occupying the binding site, so our hypothesis that a keyhole can form in this region seems plausible.

Intriguingly, the apo crystal structure shows H4/H5 crystal contacts that juxtapose the keyholes of each protein (see Figure 6). Thus our docking findings suggest a possible novel binding mode for bivalent ligands.(Dror et al., 2011; Valant, Robert Lane, Sexton, & Christopoulos, 2012)

The keyhole hypothesis does not provide a complete rationalisation of the β_1-AR selectivity for all extended ligands, as both β_1- and β_2-AR subtypes appear capable of producing this feature. However there are subtle differences between subtypes in the geometry and chemical composition of the keyhole due to the non-conserved Val/Thr$^{4.56}$. Previous studies on the potential impact of the β_2 Thr$^{186\ 4.56}$Ile genetic polymorphism have argued that this mutation will impact on water-mediated hydrogen bonding between Ser$^{165,4.55}$, Ser$^{207,5.46}$ and this amino acid, making the interactions in this region more similar to those in β_1-AR(Warne et al., 2011). Intriguingly, a water molecule can be found in or near to the keyhole region of several of the current β_1-AR XRC structures to date. (Christopher et al., 2013; Miller-Gallacher et al., 2014; Warne et al., 2012)

How these findings can be used to rationalise β-AR SAR remains to be fully explored. It is known that subtype selectivity involves a complex cross talk between features in both the head and tail moieties. It may be that slight differences in how the molecules occupy the pocket, enforced by the constraints of the narrow keyhole region, alter the effectiveness of interactions between the tail extensions and key functional groups in the receptors. The current understanding is that the mechanism by which ligands enter the β-ARs is different between subytpes.(Dror et al., 2011) This is likely the case, when they share such conserved binding pockets but show such diverse pharmacology for ligands such as those discussed in this paper. It may be that the method by which ligands enter the β_1AR is conducive to the formation of the keyhole,

allowing extended ligands to utilise this feature on docking, or as an allosteric site. This fits with the known pharmacology, as a change in the residue lining the keyhole at position 4.56 from Val to Thr would result in a more polar keyhole region which may be occluded by water, forcing the hydrophobic head group extensions to adopt U-shaped poses rather than occupy the keyhole.

The plasticity of ligand binding sites in proteins is well appreciated and attempts to predict the modes of binding of new ligands to known receptors can depend critically on adequately sampling this. The β-ARs are no exception; at a 'micro' level, $Ser^{5.42}$, $Ser^{5.46}$ and $Asn^{6.55}$, have each been shown to adopt alternative rotamer states depending on the ligand co-crystallised.(Valant et al., 2012; Warne et al., 2011; 2012) Larger ligands, such as those studied here, can be expected to bring about more drastic adaptations in protein structure. An example can be seen when comparing the A_{2A} structures crystallised with agonists adenosine(Lebon et al., 2011; Warne et al., 2011) and UK432097,(Warne et al., 2011; 2012; Xu et al., 2011) the latter of which induced a 3.8 Å widening of the binding pocket mouth due to extracellular loop rearrangement.(Lebon et al., 2011; Tate, 2012) The ability of computational methods to predict such adaptions has obvious importance when crystal structures remain, at times, elusive, and additionally is a valuable resource when there is a wish to think "outside the box" of existing structural data for the design of novel ligands.

Author Contributions

ALE performed all computational experiments. ALE, CAL, BK and PMF contributed to experimental design. CAL developed the NAB implementation of ASP. The manuscript was written through contributions of all authors. All authors have given approval to the final version of the manuscript.

Funding Sources

We acknowledge financial support from the Royal Pharmaceutical Society (formally Royal Pharmaceutical Society of Great Britain) through provision of an Academic Excellence Award (AE).

Orcid

Abigail L. Emtage http://orcid.org/0000-0001-7763-0076

Shailesh N. Mistry http://orcid.org/0000-0002-2252-1689

Peter M. Fischer http://orcid.org/0000-0002-5866-9271

Barrie Kellam http://orcid.org/0000-0003-0030-9908

Charles A. Laughton http://orcid.org/0000-0003-4090-3960

References

Baker, J. G. (2005). The selectivity of β-adrenoceptor antagonists at the human β1, β2 and β3 adrenoceptors. *British Journal of Pharmacology*, *144*(3), 317–322. http://doi.org/10.1038/sj.bjp.0706048

Baker, J. G. (2010). A full pharmacological analysis of the three turkey β-adrenoceptors and comparison with the human β-adrenoceptors. *PLoS ONE*, *5*(11), e15487. http://doi.org/10.1371/journal.pone.0015487.t005

Baker, J. G., Proudman, R. G. W., & Tate, C. G. (2011). The pharmacological effects of the thermostabilising (m23) mutations and intra and extracellular (β36) deletions essential for crystallisation of the turkey β-adrenoceptor. *Naunyn-Schmiedeberg's Archives of Pharmacology*, *384*(1), 71–91. http://doi.org/10.1007/s00210-011-0648-4

Baker, J. G., Proudman, R. G. W., Hawley, N. C., Fischer, P. M., & Hill, S. J. (2008). Role of key transmembrane residues in agonist and antagonist actions at the two conformations of the human beta1-adrenoceptor. *Molecular Pharmacology*, *74*(5), 1246–1260. http://doi.org/10.1124/mol.108.048371

Ballesteros, J. A., & Weinstein, H. (1995). [19] Integrated methods for the construction of three-dimensional models and computational probing of structure-function relations in G protein-coupled receptors. In *Methods in Neurosciences* (Vol. 25, pp. 366–428). Elsevier. http://doi.org/10.1016/S1043-9471(05)80049-7

Benfield, P., & Sorkin, E. M. (1987). Esmolol: a preliminary review of its

pharmacodynamic and pharmacokinetic properties, and therapeutic efficacy. *Drugs*, *33*(4), 392–412.

Bokoch, M. P., Zou, Y., Rasmussen, S. G. F., Liu, C. W., Nygaard, R., Rosenbaum, D. M., Fung, J. J., Choi1, H. J., Thian, F. S., Kobilka, T. S., Puglisi, J. D., Weis, W. I., Pardo, L., Prosser, R. S., Mueller, L., & Kobilka, B. K. (2010). Ligand-specific regulation of the extracellular surface of a G-protein-coupled receptor. *Nature*, *463*(7277), 108–112. http://doi.org/10.1038/nature08650

Case, D. A., Cheatham, T. E., Darden, T., Gohlke, H., Luo, R., Merz, K. M., Onufriev, A., Simmerling, C., Wang, B., & Woods, R. J. (2005). The Amber biomolecular simulation programs. *Journal of Computational Chemistry*, *26*(16), 1668–1688. http://doi.org/10.1002/jcc.20290

Chelikani, P., Hornak, V., Eilers, M., Reeves, P. J., Smith, S. O., RajBhandary, U. L., & Khorana, H. G. (2007). Role of group-conserved residues in the helical core of beta2-adrenergic receptor. *Proceedings of the National Academy of Sciences*, *104*(17), 7027–7032. http://doi.org/10.1073/pnas.0702024104

Cherezov, V., Rosenbaum, D. M., Hanson, M. A., Rasmussen, S. G. F., Thian, F. S., Kobilka, T. S., Choi, H-J., Kuhn, P., Weis, W. I., Kobilka, B. K., & Stevens, R. C. (2007). High-Resolution Crystal Structure of an Engineered Human 2-Adrenergic G Protein Coupled Receptor. *Science*, *318*(5854), 1258–1265. http://doi.org/10.1126/science.1150577

Christopher, J. A., Brown, J., Doré, A. S., Errey, J. C., Koglin, M., Marshall, F. H., Myszka, D. G., Rich, R. L., Tate, C. G., Tehan, B., Warne, T., Congreve, M. (2013). Biophysical Fragment Screening of the β 1-Adrenergic Receptor: Identification of High Affinity Arylpiperazine Leads Using Structure-Based Drug Design. *Journal of Medicinal Chemistry*, *56*(9), 3446–3455. http://doi.org/10.1021/jm400140q

Congreve, M., Langmead, C. J., Mason, J. S., & Marshall, F. H. (2011). Progress in structure based drug design for G protein-coupled receptors. *Journal of Medicinal Chemistry*, *54*(13), 4283–4311. http://doi.org/10.1021/jm200371q

Davis, I. W., Leaver-Fay, A., Chen, V. B., Block, J. N., Kapral, G. J., Wang, X., Murray, L. W., Arendall III, W. B., Snoeyink, J., Richardson, J. S., & Richardson. D. C. (2007). MolProbity: all-atom contacts and structure validation for proteins and nucleic acids. *Nucleic Acids Research*, *35*(Web Server issue), 375–383. http://doi.org/10.1093/nar/gkm216

Dixon, R. A., Sigal, I. S., Candelore, M. R., Register, R. B., Scattergood, W., Rands, E., & Strader, C. D. (1987). Structural features required for ligand binding to the beta-adrenergic receptor. *The EMBO Journal*, *6*(11), 3269–3275.

Dror, R. O., Pan, A. C., Arlow, D. H., Borhani, D. W., Maragakis, P., Shan, Y., Xu, H., & Shaw, D. E. (2011). Pathway and mechanism of drug binding to G-protein-coupled receptors. *P Proceedings of the National Academy of Sciences*, *108*(32), 13118–13123. http://doi.org/10.1073/pnas.1104614108

Fahmy, K., Jager, F., Beck, M., Zvyaga, T. A., Sakmar, T. P., & Siebert, F. (1993). Protonation states of membrane-embedded carboxylic-acid groups in rhodopsin and metarhodopsin-II – A Fourier-transform infrared spectroscopy study of site-directed mutants. *Proceedings of the National Academy of Sciences, 90,* 10206-10210.

Friesner, R. A., Banks, J. L., Murphy, R. B., Halgren, T. A., Klicic, J. J., Mainz, D. T., Repasky, M. P., Knoll, E. H., Shelley, M., Perry, J. K., Shaw, D. E., Francis, P., & Shenkin, P. S. (2004). Glide: A New Approach for Rapid, Accurate Docking and Scoring. 1. Method and Assessment of Docking Accuracy. *Journal of Medicinal Chemistry*, *47*(7), 1739–1749. http://doi.org/10.1021/jm0306430

González, A., Perez-Acle, T., Pardo, L., & Deupi, X. (2011). Molecular basis of ligand dissociation in β-adrenergic receptors. *PLoS ONE*, *6*(9), e23815. http://doi.org/10.1371/journal.pone.0023815

Green, S. A., Cole, G., Jacinto, M., Innis, M., & Liggett, S. B. (1993). A polymorphism of the human beta 2-adrenergic receptor within the fourth transmembrane domain alters ligand binding and functional properties of the receptor. *The Journal of Biological Chemistry*, *268*(31), 23116–23121.

Green, S. A., Rathz, D. A., Schuster, A. J., & Liggett, S. B. (2001). The Ile164 β2-adrenoceptor polymorphism alters salmeterol exosite binding and conventional agonist coupling to Gs. *European Journal of Pharmacology*, *421*(3), 141–147. http://doi.org/10.1016/S0014-2999(01)01049-4

Hanson, M. A., Cherezov, V., Griffith, M. T., Roth, C. B., Jaakola, V.-P., Chien, E. Y. T., Velasquez, J., Kuhn, P., & Stevens, R. C. (2008). A Specific Cholesterol Binding Site Is Established by the 2.8 Å Structure of the Human β2-Adrenergic Receptor. *Structure*, *16*(6), 897–905. http://doi.org/10.1016/j.str.2008.05.001

Heifetz, A., Schertler, G. F. X., Seifert, R., Tate, C. G., Sexton, P. M., Gurevich, V. V., Fourmy, D., Cherezov, V., Marshall, F. H., Storer, R. I., Moraes, I., Tikhonova, I. G., Tautermann, C. S., Hunt, P., Ceska, T., Hodgson, S., Bodkin, M. J., Singh, S., Law, R. J., & Biggin, P. C. (2015). GPCR structure, function, drug discovery and crystallography: report from Academia-Industry International Conference (UK Royal Society) Chicheley Hall, 1-2 September 2014. *Naunyn-Schmiedeberg's Archives of Pharmacology*, *388*(8), 883–903. http://doi.org/10.1007/s00210-015-1111-8

Hildebrand, P. W., Scheerer, P., Park, J. H., Choe, H.-W., Piechnick, R., Ernst, O. P., et al. (2009). A ligand channel through the G protein coupled receptor opsin. *PLoS ONE*, *4*(2), e4382. http://doi.org/10.1371/journal.pone.0004382

Hornak, V., Abel, R., Okur, A., Strockbine, B., Roitberg, A., & Simmerling, C. (2006). Comparison of multiple Amber force fields and development of improved protein backbone parameters. *Proteins: Structure, Function, and Bioinformatics*, *65*(3), 712–725. http://doi.org/10.1002/prot.21123

Huang, J., Chen, S., Zhang, J. J., & Huang, X.-Y. (2013). Crystal structure of oligomeric β1-adrenergic G protein-coupled receptors in ligand-free basal state. *Nature Structural & Molecular Biology*, *20*(4), 419–425. http://doi.org/10.1038/nsmb.2504

Jacobson, M. P., Friesner, R. A., Xiang, Z., & Honig, B. (2002). On the role of the crystal environment in determining protein side-chain conformations. *Journal of Molecular Biology*, *320*(3), 597–608.

Jacobson, M. P., Pincus, D. L., & Rapp, C. S. (2004). A hierarchical approach to all-atom protein loop prediction - Jacobson - 2004 - Proteins: Structure, Function, and Bioinformatics - Wiley Online Library. *Proteins: Structure, Function, and Bioinformatics*, *55*, 351–367.

Jakalian, A., Bush, B. L., Jack, D. B., & Bayly, C. I. (2000). Fast, efficient generation of high-quality atomic charges. AM1-BCC model: I. Method. *Journal of Computational Chemistry*, *21*(2), 132–146. http://doi.org/10.1002/(SICI)1096-987X(20000130)21:2<132::AID-JCC5>3.0.CO;2-P

Jakalian, A., Jack, D. B., & Bayly, C. I. (2002). Fast, efficient generation of high-quality atomic charges. AM1-BCC model: II. Parameterization and validation. *Journal of Computational Chemistry*, *23*(16), 1623–1641. http://doi.org/10.1002/jcc.10128

Katritch, V., Cherezov, V., & Stevens, R. C. (2012). Diversity and modularity of G

protein-coupled receptor structures. *Trends in Pharmacological Sciences*, *33*(1), 17–27. http://doi.org/10.1016/j.tips.2011.09.003
Kobilka, B. K. (2007). G protein coupled receptor structure and activation. *Biochim Biophys Acta*, *1768*(4), 794–807. http://doi.org/10.1016/j.bbamem.2006.10.021
Kobilka, B. K. (2011). Structural insights into adrenergic receptor function and pharmacology. *Trends in Pharmacological Sciences*, *32*(4), 213–218. http://doi.org/10.1016/j.tips.2011.02.005
Larkin, M. A., Blackshields, G., Brown, N. P., Chenna, R., McGettigan, P. A., McWilliam, H., Valentin, F., Wallace, I. M., Wilm, A., Lopez, R., Thompson, J. D., Gibson, T. J., & Higgins, D. G.. (2007). Clustal W and Clustal X version 2.0. *Bioinformatics*, *23*(21), 2947–2948. http://doi.org/10.1093/bioinformatics/btm404
Laskowski, R. A., MacArthur, M. W., Moss, D. S., & Thornton, J. M. (1993). PROCHECK: a program to check the stereochemical quality of protein structures. *Journal of Applied Crystallography*, *26*(2), 283–291. http://doi.org/10.1107/S0021889892009944
Lebon, G., Warne, T., & Tate, C. G. (2012). Agonist-bound structures of G protein-coupled receptors. *Current Opinion in Structural Biology*, *22*(4), 482–490. http://doi.org/10.1016/j.sbi.2012.03.007
Lebon, G., Warne, T., Edwards, P. C., Bennett, K., Langmead, C. J., Leslie, A. G. W., & Tate, C. G. (2011). Agonist-bound adenosine A2A receptor structures reveal common features of GPCR activation. *Nature*, *474*(7352), 521–525. http://doi.org/doi:10.1038/nature10136
Liu, J. J., Horst, R., Katritch, V., Stevens, R. C., & Wuthrich, K. (2012). Biased Signaling Pathways in β2-Adrenergic Receptor Characterized by 19F-NMR. *Science*, *335*(6072), 1106–1110. http://doi.org/10.1126/science.1215802
Louis, S. N. S., Nero, T. L. T., Iakovidis, D. D., Jackman, G. P. G., & Louis, W. J. W. (1999). LK 204-545, a highly selective beta1-adrenoceptor antagonist at human beta-adrenoceptors. *European Journal of Pharmacology*, *367*(2-3), 431–435. http://doi.org/10.1016/S0014-2999(99)00019-9
Macke, T. J., & Case, D. A. (2009). Modeling unusual nucleic acid structures. *Journal of the American Chemical Society*, *682*, 379–393. http://doi.org/10.1021/bk-1998-0682.ch024
Miller-Gallacher, J. L., Nehmé, R., Warne, T., Edwards, P. C., Schertler, G. F. X., Leslie, A. G. W., & Tate, C. G. (2014). The 2.1 Å resolution structure of cyanopindolol-bound β1-adrenoceptor identifies an intramembrane Na^+ ion that stabilises the ligand-free receptor. *PLoS ONE*, *9*(3), e92727. http://doi.org/10.1371/journal.pone.0092727.s009
Mistry, S. N., Baker, J. G., Fischer, P. M., Hill, S. J., Gardiner, S. M., & Kellam, B. (2013). Synthesis and in vitro and in vivo characterization of highly β1-Selective β-adrenoceptor partial agonists. *Journal of Medicinal Chemistry*, *56*(10), 3852–3865. http://doi.org/10.1021/jm400348g
Moukhametzianov, R., Warne, T., Edwards, P. C., Serrano-Vega, M. J., Leslie, A. G., Tate, C. G., & Schertler, G. F. (2011). Two distinct conformations of helix 6 observed in antagonist-bound structures of a β1-adrenergic receptor. *Proceedings of the National Academy of Sciences*, *108*(20), 8228–8232.
National Center for Biotechnology Information. Protein Database. Retrieved August 26, 2013, from http://www.ncbi.nlm.nih.gov/protein
Onufriev, A., Bashford, D., & Case, D. A. (2000). Modification of the generalized born model suitable for macromolecules. *The Journal of Physical Chemistry B*, *104*(15), 3712–3720. http://doi.org/10.1021/jp994072s

Onufriev, A., Bashford, D., & Case, D. A. (2004). Exploring protein native states and large-scale conformational changes with a modified generalized born model. *Proteins: Structure, Function, and Bioinformatics*, *55*(2), 383–394. http://doi.org/10.1002/prot.20033

Parrill, A. L., & Bautista, D. L. (2010). GPCR conformations: implications for rational drug design. *Pharmaceuticals*, *4*(1), 7–43. http://doi.org/10.3390/ph4010007

Pearlman, D. A., Case, D. A., Caldwell, J. W., Ross, W. S., Cheatham, T. E., III, DeBolt, S., Ferguson, D., Seibel, G., & Kollman, P. (1995). AMBER, a package of computer programs for applying molecular mechanics, normal mode analysis, molecular dynamics and free energy calculations to simulate the structural and energetic properties of molecules. *Computer Physics Communications*, *91*(1-3), 1–41. http://doi.org/10.1016/0010-4655(95)00041-D

Rasmussen, S. G. F., Choi, H.-J., Rosenbaum, D. M., Kobilka, T. S., Thian, F. S., Edwards, P. C., Burghammer, M., Ratnala, V. R. P., Sanishvili, R., Fischetti, R. F., Schertler, G. F. X., Weis, W. I., & Kobilka, B. K. (2007). Crystal structure of the human β2 adrenergic G-protein-coupled receptor. *Nature*, *450*(7168), 383–387. http://doi.org/10.1038/nature06325

Rasmussen, S. G. F., Choi, H.-J., Fung, J. J., Pardon, E., Casarosa, P., Chae, P. S., DeVree, B. T., Rosenbaum, D. M., Thian, F. S., Kobilka, T.S., Schnapp, A., Konetzki, I., Sunahara, R. K., Gellman, S. H., Pautsch, A., Steyaert, J.,Weis, W. I., & Kobilka, B. K. (2011a). Structure of a nanobody-stabilized active state of the β2 adrenoceptor. *Nature*, *469*(7329), 175–180. http://doi.org/10.1038/nature09648

Rasmussen, S. G. F., DeVree, B. T., Zou, Y., Kruse, A. C., Chung, K. Y., Kobilka, T. S., Thian, F. S., Chae, P. S., Pardon, E., Calinski, D., Mathiesen, J. M., Shah, S. T. A., Lyons, J. A., Caffrey, M., Gellman, S. H., Steyaert, J., Skiniotis, G., Weis, W. I., Sunahara, R. K., & Kobilka, B. K. (2011b). Crystal structure of the β2 adrenergic receptor-Gs protein complex. *Nature*, *477*(7366), 549–555. http://doi.org/10.1038/nature10361

Ring, A. M., Manglik, A., Kruse, A. C., Enos, M. D., Weis, W. I., Garcia, K. C., & Kobilka, B. K. (2014). Adrenaline-activated structure of beta2-adrenoceptor stabilised by an engineered nanobody. *Nature*, *502*(7472), 575–579. http://doi.org/10.1038/nature12572

Rosenbaum, D. M., Zhang, C., Lyons, J. A., Holl, R., Aragao, D., Arlow, D. H., Rasmussen, S. G. F., Choi, H-J., DeVree, B. T., Sunahara, R. K., Chae, P. S., Gellman, S. H., Dror, R. O., Shaw, D. E.,Weis, W. I., Caffrey, M., Gmeiner, P., & Kobilka, B. K. (2011). Structure and function of an irreversible agonist-β2 adrenoceptor complex. *Nature*, *469*(7329), 236–240. http://doi.org/10.1038/nature09665

Selvam, B., Wereszczynski, J., & Tikhonova, I. G. (2012). Comparison of dynamics of extracellular accesses to the β1 and β2 adrenoceptors binding sites uncovers the potential of kinetic basis of antagonist selectivity. *Chemical Biology & Drug Design*, *80*(2), 215–226. http://doi.org/10.1111/j.1747-0285.2012.01390.x

Strader, C. D., Sigal, I. S., Candelore, M. R., Rands, E., Hill, W. S., & Dixon, R. A. (1988). Conserved aspartic acid residues 79 and 113 of the beta-adrenergic receptor have different roles in receptor function. *The Journal of Biological Chemistry*, *263*, 10267–10271.

Strader, C. D., Sigal, I. S., Register, R. B., Candelore, M. R., Rands, E., & Dixon, R. A. (1987). Identification of residues required for ligand binding to the beta-adrenergic receptor. *Proceedings of the National Academy of Sciences*. *84*(13), 4384-8.

Strosberg, A. D. (1993). Structure, function, and regulation of adrenergic receptors.

Protein Science : a Publication of the Protein Society, *2*(8), 1198–1209. http://doi.org/10.1002/pro.5560020802
Suite 2012: Glide, version 5.8, Schrödinger, LLC, New York, NY, 2012.
Suite 2012: LigPrep, version 2.5, Schrödinger, LLC, New York, NY, 2012.
Suite 2012: Maestro, version 9.3, Schrödinger, LLC, New York, NY, 2012.
Suite 2012: Prime, version 3.1, Schrödinger LLC New York, NY, 2012.
Tate, C. G. (2012). A crystal clear solution for determining G-protein-coupled receptor structures. *Trends Biochemical Sciences*, *37*(9), 343–352. http://doi.org/10.1016/j.tibs.2012.06.003
The PyMOL Molecular Graphics System, version 1.5.0.4, Schrödinger, LLC.
Topiol, S., & Sabio, M. (2009). X-ray structure breakthroughs in the GPCR transmembrane region. *Biochemical Pharmacology*, *78*, 11–20.
Valant, C., Robert Lane, J., Sexton, P. M., & Christopoulos, A. (2012). The best of both worlds? Bitopic orthosteric/allosteric ligands of G protein–coupled receptors. *Annual Review of Pharmacology and Toxicology*, *52*(1), 153–178. http://doi.org/10.1146/annurev-pharmtox-010611-134514
Vanni, S., Neri, M., Tavernelli, I., & Rothlisberger, U. (2009). Observation of "ionic lock" formation in molecular dynamics simulations of wild-type β1 and β2 adrenergic receptors. *Biochemistry*, *48*(22), 4789–4797. http://doi.org/10.1021/bi900299f
Vanni, S., Neri, M., Tavernelli, I., & Rothlisberger, U. (2011). Predicting novel binding modes of agonists to β adrenergic receptors using all-atom molecular dynamics dimulations. *PLoS Computational Biology*, *7*(1), e1001053. http://doi.org/10.1371/journal.pcbi.1001053
Venkatakrishnan, A. J., Deupi, X., Lebon, G., Tate, C. G., Schertler, G. F., & Babu, M. M. (2013). Molecular signatures of G-protein-coupled receptors. *Nature*, *494*(7436), 185–194. http://doi.org/10.1038/nature11896
Wacker, D., Fenalti, G., Brown, M. A., Katritch, V., Abagyan, R., Cherezov, V., & Stevens, R. C. (2010). Conserved binding mode of human β2-adrenergic receptor inverse agonists and antagonist revealed by X-ray crystallography. *Journal of the American Chemical Society*, *132*(33), 11443–11445. http://doi.org/10.1021/ja105108q
Wang, J., Wang, W., Kollman, P. A., & Case, D. A. (2005). Antechamber: an accessory software package for molecular mechanical calculations. *Journal of Computational Chemistry*, *25*, 1157–1174.
Wang, T., & Duan, Y. (2007). Chromophore channeling in the G-protein coupled receptor rhodopsin. *Journal of the American Chemical Society*, *129*(22), 6970–6971. http://doi.org/10.1021/ja0691977
Wang, T., & Duan, Y. (2009). Ligand entry and exit pathways in the β2-adrenergic receptor. *Journal of Molecular Biology*, *392*(4), 1102–1115. http://doi.org/10.1016/j.jmb.2009.07.093
Warne, T., Edwards, P. C., Leslie, A. G. W., & Tate, C. G. (2012). Crystal Structures of a Stabilized beta1-Adrenoceptor Bound to the Biased Agonists Bucindolol and Carvedilol. *Structure*, *20*(5), 841–849. http://doi.org/10.1016/j.str.2012.03.014
Warne, T., Moukhametzianov, R., Baker, J. G., Nehmé, R., Edwards, P. C., Leslie, A. G. W., Schertler, G. F. X., & Tate, C. G. (2011). The structural basis for agonist and partial agonist action on a β1-adrenergic receptor. *Nature*, *469*(7329), 241–244. http://doi.org/10.1038/nature09746
Warne, T., Serrano-Vega, M. J., Baker, J. G., Moukhametzianov, R., Edwards, P. C., Henderson, R., Leslie, A. G. W., Tate, C. G., & Schertler, G. F. X. (2008). Structure

of a β1-adrenergic G-protein-coupled receptor. *Nature*, *454*(7203), 486–491. http://doi.org/10.1038/nature07101

Weichert, D., Kruse, A. C., Manglik, A., Hiller, C., Zhang, C., Hübner, H., Kobilka, B. K., & Gmeiner, P. (2014). Covalent agonists for studying G protein-coupled receptor activation. *Proceedings of the National Academy of Sciences of the United States of America*, *111*(29), 10744–10748. http://doi.org/10.1073/pnas.1410415111

Withers, I. M., Mazanetz, M. P., Wang, H., Fischer, P. M., & Laughton, C. A. (2008). Active site pressurization: a new tool for structure-guided drug design and other studies of protein flexibility. *Journal of Chemical Information and Modeling*, *48*(7), 1448–1454. http://doi.org/10.1021/ci7004725

Xu, F., Wu, H., Katritch, V., Han, G. W., Jacobson, K. A., Gao, Z.-G., Cherezov, V., & Stevens, R. C. (2011). Structure of an agonist-bound human A2A adenosine receptor. *Science*, *332*(6027), 322–327. http://doi.org/10.1126/science.1202793

Zou, Y., Weis, W. I., & Kobilka, B. K. (2012). N-terminal T4 lysozyme fusion facilitates crystallization of a G protein coupled receptor. *PLoS ONE*, *7*(10), e46039. http://doi.org/10.1371/journal.pone.0046039

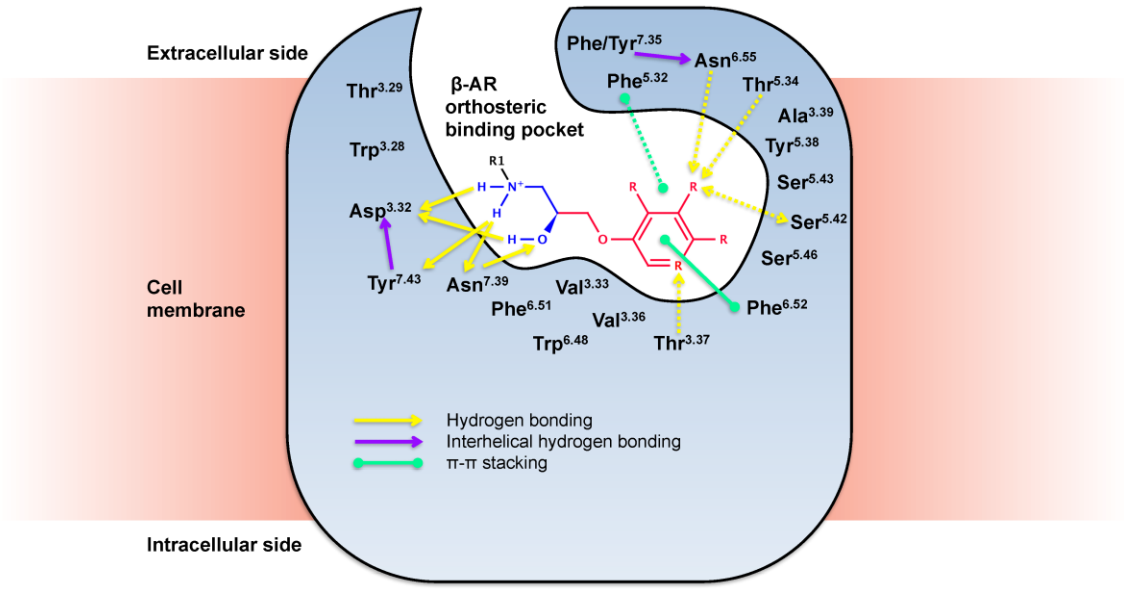

Figure 1. Schematic of the conventional β-AR antagonist ligand-binding site. The orthosteric binding pockets of β_1- and β_2-ARs are almost identical. Residues within 4 Å of an antagonist ligand template are shown. The only difference evident is at position 7.35 (Ballesteros-Weinstein numbering), where Phe^{359} in β_1-AR is replaced by Tyr^{308} in β_2-AR. Dashed lines represent ligand-specific interactions (see text for details).

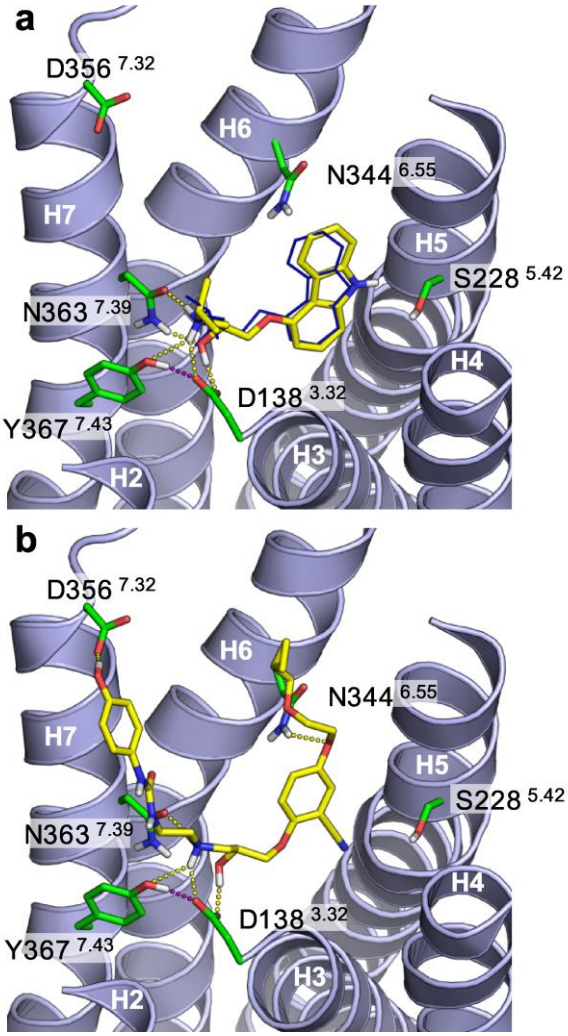

Figure 2. Conventional and U-shaped docking poses in the β_1-AR model. (a) Carazolol (**1**) (yellow) docked to the β_1-AR model (grey helices) in good agreement with the 2YCW crystal carazolol (**1**) placement (thin blue structure). (b) LK 204–545 (**16**) exhibiting a U-shaped pose with both the head and tail ends of the molecule in solvent-accessible regions. The tail group may confer selectivity by interacting with non-conserved residue $D^{356,7.32}$ ($K^{305,7.32}$ in β_2-AR). In both (a) and (b) the extracellular ends of H2 and H3 have been removed for clarity and ECL2 and H1 are not shown. Side chain and ligand carbon atoms are coloured green and yellow, respectively. Polar hydrogens are white, nitrogen atoms are coloured blue and oxygen atoms red. Potential H-bonding is indicated with yellow dashed lines with the exception of the interhelical H-bond between Tyr^{367} and Asp^{138}, which is displayed as a purple dashed line. The β_1-

AR residue numbering is displayed for highlighted polar residues with Ballesteros-Weinstein numbering in superscript.

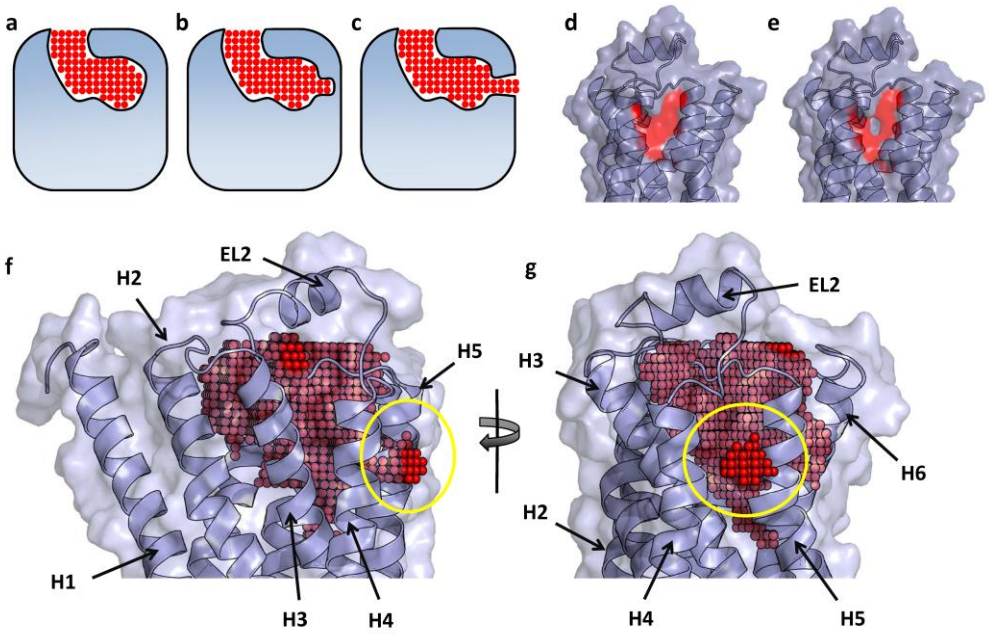

Figure 3. The Active Site Pressurisation (ASP) process. The schematics (a)–(c) represent the ASP process whereby non-charged Lennard-Jones particles (red spheres) fill up the binding pocket over the course of an MD simulation. The initial filling (a) packs the receptor (grey) cavity; it is a dynamic process so subsequent particles are added where receptor plasticity exists (b). Side chains continue to move creating further space for particles to fill; in some cases channels are formed (c). (d) Shows the β_1-AR model surface of H4 and H5 before ASP, (e) is the same view after ASP and depicts the size and location of the keyhole. The residues Tyr$^{5.38}$, Ser$^{5.42}$, Ser$^{5.46}$, Val$^{4.56}$ and Pro$^{4.50}$, which line the keyhole, are coloured red in both cases. (f) Shows the β_1-AR model in the final stages of the ASP process and the red Lennard–Jones particles (1.1 Å radius) protruding outwards having broken the integrity of the cavity wall between H4 and H5 (highlighted by the yellow circle). (g) Is the same as (f) but rotated about the y axis by −90° to show the location of the cavity breach.

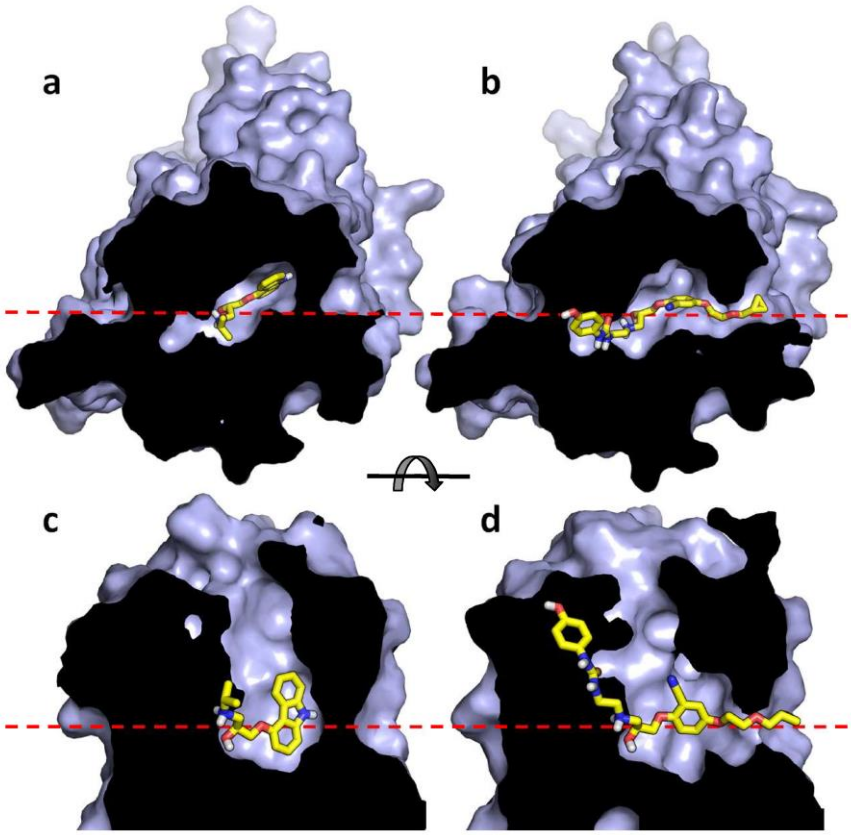

Figure 4. “Top” and “side” views of the β_1-AR cavity before and after Active Site Pressurisation and the extended head group of LK 204-545 (**16**) docked through the keyhole of the β_1-AR model. (a) and (c) show the original β_1-AR model (prior to ASP), with carazolol (**1**) docked into the pocket. (b) and (d) show the β_1-AR model after it has been subjected to ASP and a narrow fissure has formed between H4 and H5. In (a) and (b) the extracellular surface of the receptor has been clipped away to reveal the pocket shape at the depth of carazolol’s (**1**) chiral carbinol (this plane is represented by the red dashed line in (c) and (d)). (c) and (d) represent a vertical slice along the extracellular to intracellular length of the receptor (also indicated by the red dashed line in (a) and (b)). (b) and (d) show the capability of the keyhole to accommodate the extended head group of ligands such as LK 204-545 (**16**). The carbon atoms of carazolol (**1**) and LK 204-545 (**16**) are coloured yellow. Polar hydrogens are white, nitrogen atoms are blue and oxygen atoms red.

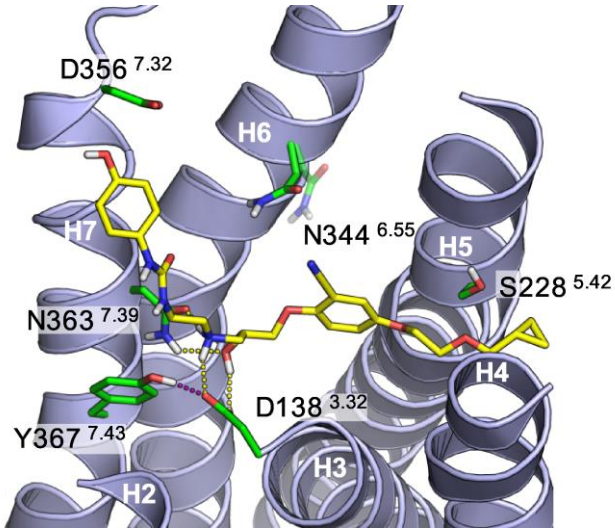

Figure 5. The extended head group of LK 204-545 (**16**) docked through the keyhole of the β_1-AR model. This figure indicates the position of LK 204-545 (**16**) in relation to key binding pocket residues. Canonical interactions are observed between the ethanolamine core of the ligand and $Asp^{3.32}$ and $Asn^{7.39}$ while the extended head group is positioned between H4 and H5 – the alkyl ether engages in polar interactions with $Ser^{5.42}$ (note new rotamer state due to ASP) while the cyclopropyl tail occupies the intra-membrane space. Colouring and representations are the same as for Figure 2. Note the vicinity of $Asn^{6.55}$ to the ligand nitrile group – if this residue were to adopt a different rotamer state (see partially transparent pre-ASP rotamer) an interaction with the ligand may be possible.

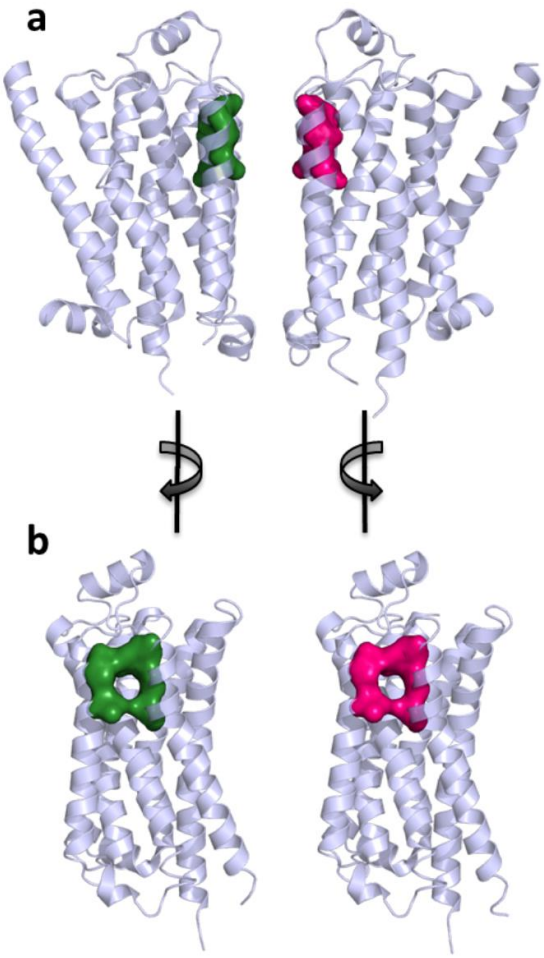

Figure 6. Aligned keyholes at the H4/H5 dimer interface found in the oligomeric ligand-free turkey β_1-AR structure. (a) Depicts the dimer interface of two turkey β_1-ARs (PDB code 4GPO; Huang et al., 2013), with keyhole residues shown in a surface representation. (b) Depicts the dimer interface opened up and each monomer rotated 90° revealing two aligned keyholes.